EXPERIMENTAL AND MODELING STUDY OF ICE MELTING

T. Kousksou[*]*, A. Jamil, Y. Zeraouli and J.-P. Dumas*

Laboratoire de Thermique Energétique et Procédés Avenue de l'Université, BP 1155, 64013 PAU Cedex, France

Differential scanning calorimetry (DSC) is applied to analyse the process of ice melting. Experimental results were compared to those obtained by a numerical simulation in which a conventional enthalpy formulation was applied. The effects of various parameters on the kinetics of transformations and therefore the shape of curves has been analysed and the importance of temperature gradients inside the sample evaluated.

Introduction

Phase change problems are encountered extensively in several practical applications areas [1–5]. Such applications include melting of ice, freezing of moist soil, crystal growth, thermal energy storage, casting of metals, thermal control of electronic equipments using phase change materials (PCMs), welding and plastic manufacturing.

For design and performance evaluation of a system contained ice, it is necessary to understand the behavior of the ice during the phase change process. Typical question are the determination of freezing and melting times.

During recent years numerical models of freezing and melting processes became increasingly interesting because of the growing availability of computer power at relatively low prices.

The most common methods used are the enthalpy method and the effective heat capacity method. The enthalpy method is introduced in many references as a numerical method for solving phase change problem [6–9]. The method has been successfully validated using both experimental and numerical data found from the literature.

The effective heat capacity approach describes both the normal specific heat of the material and the released latent heat during freezing. In this method, the latent heat effect is approximated by a large effective heat capacity over a small temperature range. It is simple in concept and easy to implement. However, it is sensitive to the choice of the phase change temperature interval and the chosen time integration scheme that non-convergence always occurs when it is implemented with implicit time integration schemes [10].

In this paper, the enthalpy formulation is used to study the kinetics of the ice melting process in the small containers (few mm^3) used into the DSC. The effects of the variation of the heating rate and the mass of sample on the melting process are presented.

Description of DSC

The principle of the power-compensation used in the DSC is that the temperatures of the sample and reference are controlled independently using separate, identical furnaces. Even in case of thermal event for the sample, the temperatures of the plates containing the sample and the reference are maintained identical. The curve is Φ the difference of power required to maintain this equality.

$$\Phi=(\Phi)_{sample}-(\Phi)_{ref} \qquad (1)$$

As indicated in [11, 12] the power exchanged at the reference plate is practically constant and equal to $(\Phi)_{ref}=\beta c_{ref}$, where c_{ref} is the specific heat of the reference cell and β is the heating rate. So to simplify the model we will omit the second term from the calculation of Φ.

Mathematical model

In Fig. 1 we have drawn the real cell and the simplified scheme used in our model. The ice is contained in a cylindrical cell of height $Z_0=1.1$ mm and radius $R=2.125$ mm.

To analyse the process of ice melting, the following assumptions have been made:

———————
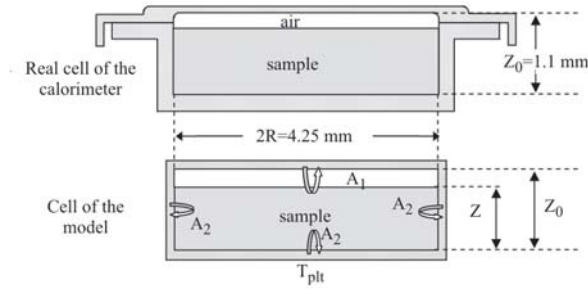[*]   Author for correspondence: tarik.kousksou@univ-pau.fr

Fig. 1 Experiment cell and scheme of the model

- The sample is regarded as a homogeneous material. The ice consists of pure water.
- Due to the small dimensions of the sample, the convection effects due to density change at the phase change interface are neglected.
- The thermophysical properties of ice and water are practically constant.

The numerical study of melting water has been conducted on a fixed-grid by using an enthalpy formulation [13, 14]. One of the advantages of the fixed-grid method is that a unique set of equations and boundary conditions is used for the whole domain, including both solid and liquid phase. In this formulation, the latent heat evolution can be illustrated by using heat conduction controlled phase change problems [15].

$$\frac{\partial[\rho h]}{\partial t}=\nabla\cdot(\lambda\nabla T) \qquad (2)$$

where λ is a mixture conductivity defined as

$$\lambda=f_{\mathrm{w}}\lambda_{\mathrm{w}}+(1-f_{\mathrm{w}})\lambda_{\mathrm{ic}} \qquad (3)$$

and is a mixture volumetric enthalpy given as

$$[\rho h]=f_{\mathrm{w}}\rho_{\mathrm{w}}\lambda_{\mathrm{w}}+(1-f_{\mathrm{w}})\rho_{\mathrm{ic}}\lambda_{\mathrm{ic}} \qquad (4)$$

where ρ_{ic} and ρ_{w} are the ice and water volume densities, h_{ic} and h_{w} are the ice and water mass enthalpy and f_{w} the water fraction.

The enthalpy of water and ice can be evaluated from a heat balance performed on the ice–water mixture by using as reference the enthalpy of the water at 0°C ($h_{\mathrm{l,T=0°C}}=0$ kJ kg^{-1}).

$$h_{\mathrm{ic}}=-L_{\mathrm{f}}+\int_0^T c_{\mathrm{ic}}(\theta)\mathrm{d}\theta \qquad (5)$$

$$h_{\mathrm{w}}=\int_0^T c_{\mathrm{w}}(\theta)\mathrm{d}\theta \qquad (6)$$

where c_{ic} and c_{w} are the ice and water mass heat capacity and L_{f} is the melting heat of ice.

Substitution of Eqs (4–6) into Eq. (2) leads to the temperature-source based energy equation used in this work

$$\frac{\partial[\rho cT]}{\partial t}=\nabla(\lambda\nabla T)-\rho_{\mathrm{ic}}L_{\mathrm{f}}\frac{\partial fw}{\partial t} \qquad (7)$$

where

$$\rho c=f_{\mathrm{w}}\rho_{\mathrm{w}}c_{\mathrm{w}}+(1-f_{\mathrm{w}})\rho_{\mathrm{ic}}c_{\mathrm{ic}} \qquad (8)$$

Initial and boundary conditions

Due to the higher thermal conductivity of the cell metal, it is assumed that the envelope of the sample is at the plate temperature.

A slip boundary condition is imposed on the symmetry axis:

$$\left(\frac{\partial T}{\partial r}\right)_{r=0}=0 \qquad (9)$$

To take into account the air between the sample and the cover of the cell (Fig. 1), we consider two different heat exchange coefficients: A_1 the heat transfer between the solution and the air in the top of the cell and A_2 the heat transfer between the sample and both lateral and bottom surface areas of the cell.

$$-\lambda\left(\frac{\partial T}{\partial r}\right)_{z=Z}=A_1(T_{z=Z}-T_{\mathrm{plt}}) \qquad (10)$$

$$-\lambda\left(\frac{\partial T}{\partial r}\right)_{r=R}=A_1(T_{r=R}-T_{\mathrm{plt}}) \qquad (11)$$

$$-\lambda\left(\frac{\partial T}{\partial r}\right)_{z=0}=A_2(T_{z=0}-T_{\mathrm{plt}}) \qquad (12)$$

where T_{plt} is the temperature of the plates, is programmed to be linear function

$$T_{\mathrm{plt}}=\beta t+T_0 \qquad (13)$$

where T_0 is the temperature of the phase at $t=0$.

The flow Φ that leaves the sample is the sum of the thermal fluxes through the walls of the metallic cell

$$\Phi=-2\pi R\int_{z=0}^{z=Z}A_2(T_{r=R}-T_{\mathrm{plt}})\mathrm{d}z-$$

$$2\pi\int_{r=0}^{r=R}A_2(T_{z=0}-T_{\mathrm{plt}})r\mathrm{d}r \qquad (14)$$

$$-2\pi\int_{r=0}^{r=R}A_1(T_{z=Z}-T_{\mathrm{plt}})r\mathrm{d}r$$

Numerical procedure

The governing equation is discretised using a finite volume technique. A fully implicit method has been adopted.

At each time step the water fraction and the temperature field in Eq. (7) are solved by using an iterative procedure. At the time step $t+\Delta t$ the initial iterative fields are initialised to previous time step t then the following iterative system (15–17) is solved:

$$f_w^{m+1}=f_w^m+\frac{\rho c}{\rho_{ic}L_f}(T^{m+1}-T_f) \qquad (15)$$

Subject to the following constraint:

$$f_w^{m+1}=\begin{cases}0 & \text{if } f_w^{m+1}\prec 0 \\ 1 & \text{if } f_w^{m+1}\succ 0\end{cases} \qquad (16)$$

$$\rho c\left(\frac{T^{m+1}-T^t}{\Delta t}\right)=\nabla(\lambda\nabla T^{m+1})-\rho_{ic}L_f\left(\frac{f_w^{m+1}-f_w^t}{\Delta t}\right) \qquad (17)$$

where m is the index of the iteration level, Δt the time step discretization and T_f the phase change temperature. The steps (15–17) are repeated until

$$\left\|(f_1)_P^{m+1}-(f_1)_P^m\right\|\prec\varepsilon \text{ and } \left\|T_P^{m+1}-T_P^m\right\|\prec\varepsilon \qquad (18)$$

and typically $\varepsilon=10^{-5}$ was used.

Results and discussion

Thermal analysis were carried out using a Pyris Diamond DSC of Perkin-Elmer. The temperature scale of the instrument was calibrated by the melting point of pure ice (273.15 K or 0°C) and mercure (234.32 K or –38.82°C). The DSC experiments were conducted by placing the distilled water in the aluminum DSC cell. The sample was cooled at 2°C min^{-1} until ice formed, typically at –50°C (observed as a sharp negative peak on the DSC curve). The sample was then heated from –50 to 20°C.

For the numerical calculation, we have applied the procedure described in the previous section. The values of physical characteristics required in the different equations are given in Table 1 [16–18], except the coefficients of heat exchange (A_1 and A_2) that have been determined by simulation from exploratory experiments.

A comparison of the experimental and numerical curve is given in Fig. 2. Good agreement can be seen in the results.

The advantage of the model is that it permits the calculation at each instant the total water fraction in-
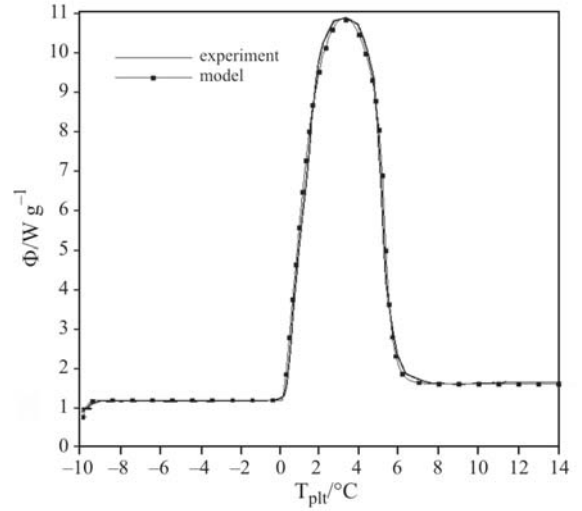

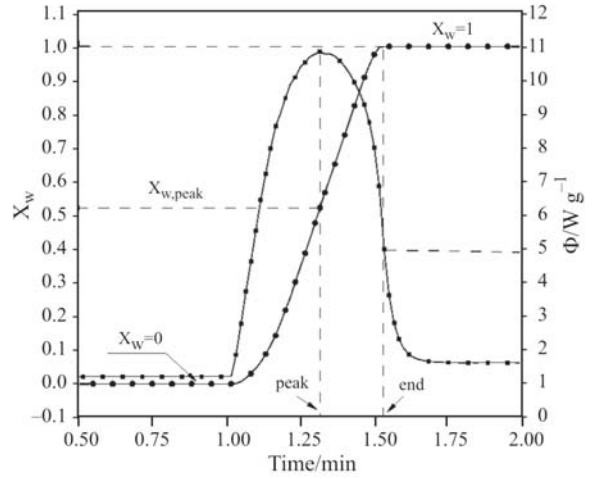**Fig. 2** Theoretical and experiment curve ($\beta=10$°C min^{-1})

Fig. 3 Total water fraction inside the sample *vs.* T_{plt}

side the sample (Fig. 3). The maximum total water fraction is 1, and this is taken as the end point of phase transformation.

Effect of the heating rate β

Figure 4 shows the curves obtained by the model and DSC *vs.* the heating rate β. The melting temperature range becomes broader and it shifts to greater temperatures with increasing heating rate.

Figure 5 shows the prediction of temperatures *vs.* T_{plt} at different point in the sample. It can be seen

Table 1 Thermophysical properties of ice and water

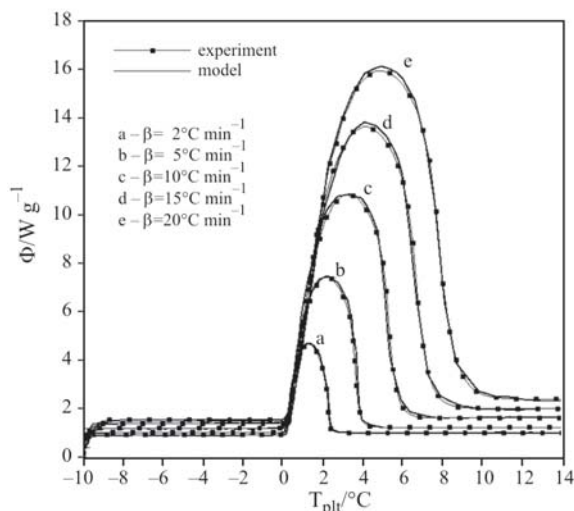|	Water	Ice
Density/kg m^{-3}	$\rho_w(T)=1000.4-0.1398\ T$	$\rho_{ic}(T)=917+0.66\cdot 10^{-2}\ T$
Thermal conductivity/W m^{-1} K^{-1}	$\lambda_w(T)=0.5580+2.06\cdot 10^{-3}\ T$	$\lambda_{ic}(T)=2.24+5.975(-T)^{1.156}$
Specific heat/kJ kg^{-1} K^{-1}	$c_w(T)=4.2058+0.9\cdot 10^{-3}\ T$	$c_{Pic}(T)=2.1162+0.78\cdot 10^{-2}\ T$

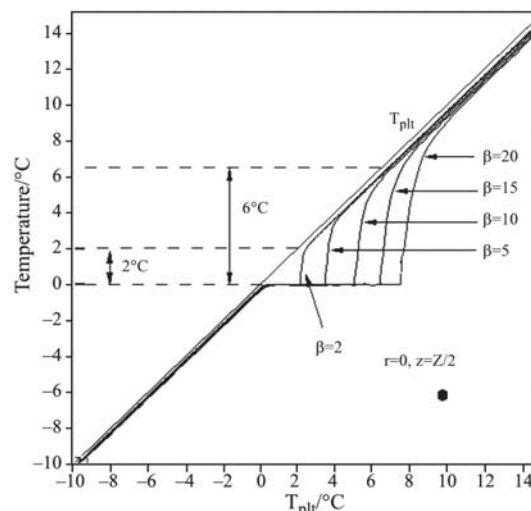**Fig. 4** Effect of the heating rate on the shape of curves

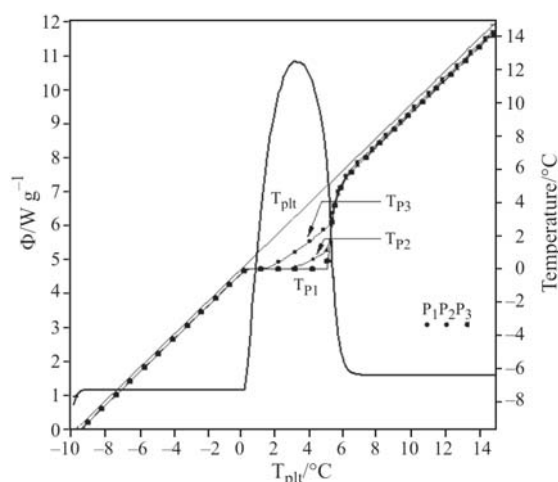**Fig. 6** Effect of the heating rate on the temperature in the center of the sample

Fig. 5 Temperature *vs.* radius (β=10°C min^{-1})

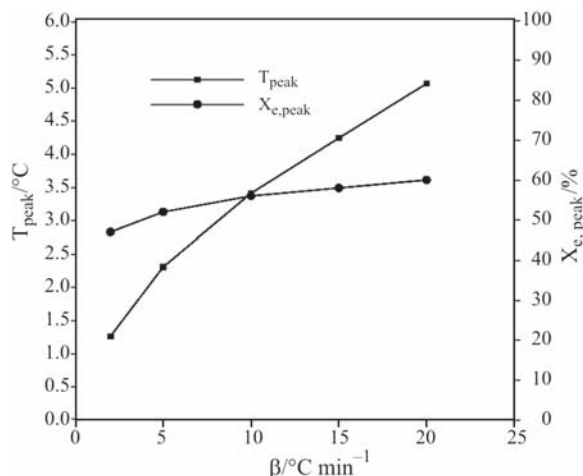**Fig. 7** T_{peak} and the corresponding total water fraction *vs.* β

from this figure that the temperature differences inside the sample can reach 2.5°C at certain points. These differences become more important as the heating rate increases Fig. 6.

Figure 7 shows a plot of the peak maximum temperature T_{peak} and the corresponding total water fraction *vs.* heating rate. We can note that the peak maximum temperature T_{peak} increase continuously and linearly with increasing heating rate. This effect on the peak temperatures is caused by the overall thermal resistance (both between the cell and the DSC plate form and within the sample). We observe that the total water fraction corresponding to the maximum of the peak increases slowly with increasing heating rate. Once the heating rate becomes lower the thermal resistance within the sample becomes negligible. In this case we can describe the kinetics of the ice melting by adopting the classical model assuming the uniformity of the sample temperature [19, 20].

Effect of the sample mass

From the numerical and experimental analysis, we present the non-normalized heat flow for different mass of the sample at a fixed heating rate, as one can see in Fig. 8. In these plots we show that both of the rising slope of curves and the peak temperature increase with increasing the sample mass. These observations can be explained principally by the resistance within the sample R_s. If we maintain the heating rate constant the overall thermal resistance should be mainly dependent on the sample mass. It is interesting to note that the ratio (area under the sharp peak/mass) remains constant ($\approx$335 kJ kg^{-1}).

From Fig. 9 we observe that the temperature difference inside sample becomes more important as the mass of sample increases. For example, the tempera-
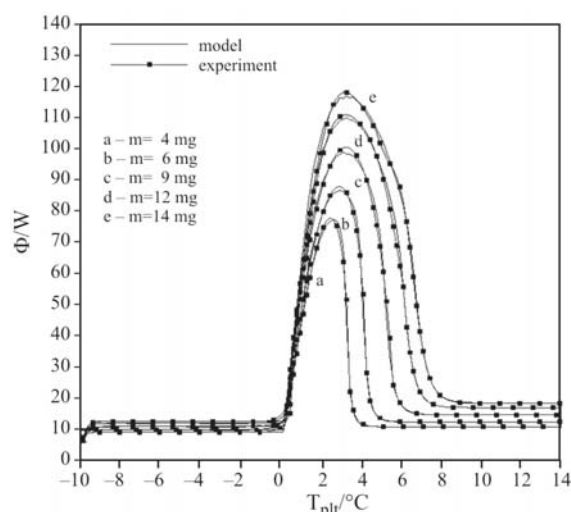
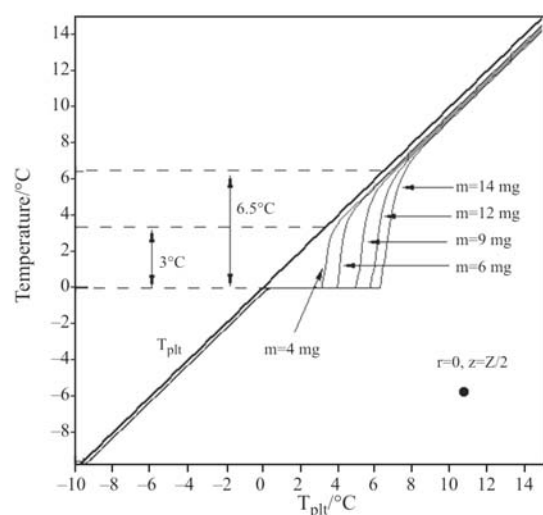**Fig. 8** Influence of the mass on the shape of curves

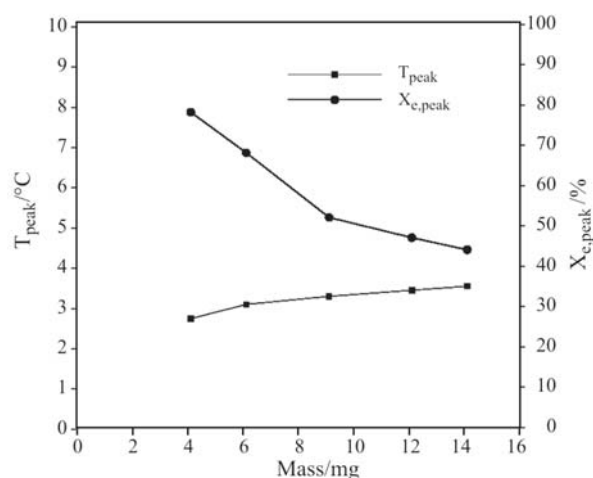**Fig. 9** Effect of the sample mass on the temperature in the center of the sample

Fig. 10 T_{peak} and the corresponding overall water fraction for different sample mass

ture difference for m=6 mg is about 3°C while for m=14 mg it is 6.5°C.

We have also presented the peak maximum temperature T_{peak} and the corresponding overall water fraction for different sample mass (Fig. 10). We observe that the overall water fraction corresponding to the maximum peak increase with decreasing the mass sample. Contrarily to the slow heating rate, in the case of the small sample mass the maximum peak correspondent approximately to the end point of the phase transformation.

Conclusions

A two-dimensional theoretical model based on the enthalpy formulation was developed to describe the ice melting in the cylindrical cell of calorimeter. Detailed analysis of the results showed that the temperature gradients inside the sample become more important if either heating rate or mass of sample increases. By employing the proposed model we can easily confirm the end point of the phase transformation. In the case of the slow heating rates, we can assume the uniformity of the sample temperature to describe the kinetics of the ice melting. With the small sample mass, the end point of the phase transformation correspondent approximately to the maximum peak.

Nomenclature

A heat transfer coefficient (W m^{-2} K^{-1})
c specific heat capacity (J kg^{-1} K^{-1})
f water fraction
h mass enthalpy (J kg^{-1})
L_f melting heat of ice (J kg^{-1})
t time (s)
T temperature (°C)

Greek symbols

β heating rate (°C min^{-1})
ΔS surface (m^2)
Δt time step (s)
λ thermal conductivity (W m^{-1} K^{-1})
ρ density (kg m^{-3})
Φ heat flow rate (W kg^{-1})

Subscripts

ic   ice
plt   plate
ref   reference
w   water

Superscripts

m   iteration level
t   previous time step value

References

 1 S. M. Hasanain, Energy Convers. Manage., 11 (1998) 1127.
 2 A. M. Khudhair and M. M. Farid, Energy Convers. Manage., 45 (2004) 263.
 3 P. Lamberg, R. Lehtiniemi and A. M. Henell, Int. J. Thermal Sci., 43 (2004) 277.
 4 A. K. Galwey, J. Therm. Anal. Cal., 82 (2005) 423.
 5 A. Ousegui, S. Zhu, H. S. Ramaswamy and A. Le Bail, J. Therm. Anal. Cal., 86 (2006) 561.
 6 V. Alexiades and A. D. Solomon, Mathematical modelling of melting and freezing processes, Hemisphere Publishing Corporation, USA 1993.
 7 G. Lane, Solar Heat Storage: Latent Heat Material, CRC Press, 1 (1983).
 8 J. Crank, Free and Moving Boundary Problems, Oxford University Press, 1984.
 9 V. Voller and M. Cross, Int. J. Heat Mass Transfer, 24 (1981) 545.
10 Z. X. Gong and A. S. Mojumdar, Int. J. Numer. Methods Heat Fluid Flow, 7 (1997) 565.
11 J. P. Dumas, Y. Zeraouli and M. Strub, Thermochim. Acta, 236 (1994) 239.
12 J. P. Dumas, Y. Zeraouli and M. Strub, Thermochim. Acta, 236 (1994) 227.
13 V. R. Voller, IMA J. Numer. Anal., 5 (1985) 201.
14 V. R. Voller and C. R. Swaminathan, Numer. Heat Transfer, 19 (1991) 175.
15 V. R. Voller, C. R. Swaminathan and B. G. Thomas, Int. J. Num. Meth. Eng., 30 (1990) 875.
16 R. H. Perry and C. H. Chilton, Chemical Engineers Handbook, New York: McGraw-Hill Book Company, 5 (1973) 1958.
17 O. Bel and A. Lallemand, Int. J. Refrigeration, 22 (1999) 164.
18 F. L. Levy, Revue International du Froid, 5 (1982) 149.
19 Y. Zeraouli, A. J. Ehmimed and J.-P. Dumas, Int. J. Thermal Sci., 39 (2000) 780.
20 T. Kousksou, A. Jamil, Y. Zeraouli and J. P. Dumas, Modčle de transferts thermiques lors de la fusion d'un corps analysé par calorimétrie ŕ balayage. JCAT 2006, Pau, 30-31 mai et 1 juin 2006.